ABSTRACT

MCGEE, LAURA CELESTE. Mesoscale and Submesoscale Mechanisms Behind Asymmetric Cooling and Phytoplankton Blooms Induced by Hurricanes: A Comparison Between an Open Ocean Case and a Continental Shelf Sea Case. (Under the direction of Dr. Ruoying He.)

Right-side bias in sea surface cooling and phytoplankton blooms is often observed in the wake of hurricanes in the Northern Hemisphere. This idealized hurricane modeling study used a coupled biological-physical model to understand the underlying mechanisms behind hurricane-induced phytoplankton bloom asymmetry. Both a deep ocean case and continental shelf sea case were considered and contrasted. Model analyses show that while right-side asymmetric mixing due to inertial oscillations and restratification from strong right-side recirculation cells contribute to bloom asymmetry in the open ocean case, the well-mixed condition in the continental shelf sea case inhibits formation of recirculation cells, and the convergence of water onto the shelf is a more important process for bloom asymmetry.

Mesoscale and Submesoscale Mechanisms Behind Asymmetric Cooling and Phytoplankton Blooms Induced by Hurricanes: A Comparison Between an Open Ocean Case and a Continental Shelf Sea Case

by
Laura Celeste McGee

A thesis submitted to the Graduate Faculty of
North Carolina State University
in partial fulfillment of the
requirements for the Degree of
Master of Science

Marine, Earth and Atmospheric Sciences

Raleigh, North Carolina

2017

APPROVED BY:

_____	_____
Dr. Ruoying He Chair of Advisory Committee	Dr. John C. Warner
_____	_____
Dr. Astrid Schnetzer	Dr. Stuart Bishop

DEDICATION

This thesis is dedicated to my family and friends. Thank you for believing in me.

BIOGRAPHY

Laura was born in Winston-Salem, NC in 1992. Early in life, she developed a love of science and fantasy/sci-fi novels, which led to an exploration of science and literature throughout secondary school. She began attending the University of North Carolina Wilmington in 2010, and decided to major in physics after taking her first physics course. She received a Bachelor of Science in physics with a double minor in biology and mathematics in 2014. After taking a year away from schooling to work with puppies, she returned for a Master's degree in 2015 at North Carolina State University.

ACKNOWLEDGMENTS

My deepest thanks to my advisor, Dr. Ruoying He, and to my committee, Dr. John Warner, Dr. Astrid Schnetzer, and Dr. Stuart Bishop. My thanks also to NASA, NOAA, Gulf of Mexico Research Initiative/GISR, and NC Sea Grant/Space Grant for their funding support. Thank you to Dr. Haibo Zong, Dr. M. Nabi Allahdadi, to Jennifer Warrillow, and to all the members of the Ocean Observing and Modeling Group, as well as to my family and friends.

TABLE OF CONTENTS

LIST OF TABLES

LIST OF FIGURES

1. INTRODUCTION

Hurricanes induce upwelling and vertical mixing along their tracks, bringing cold and nutrient-rich deep waters to the upper water column that result in significant changes in sea surface temperature (SST) and phytoplankton concentration (Price 1981, Subrahmanyam et al. 2002, Lin et al. 2003). These hurricane-induced blooms can occur even in waters that are normally oligotrophic, and thus may be an important contributor to new primary production in these sparse ecosystems (Babin et al. 2004). Studies have suggested that hurricane-induced blooms may account for 20-30% of new production, and a single hurricane event can increase primary production by an order of magnitude (Lin et al. 2003, Tsuchiya et al. 2013). These hurricane-induced blooms are rarely considered in calculations of air-sea carbon flux, and may be an important contributor (Mahadevan et al. 2011). To understand the contribution of hurricane-induced blooms to primary production and carbon flux, their main mechanisms must be understood.

As the most unique biological feature, the right-side asymmetry of phytoplankton blooms in the Northern Hemisphere has often been observed and attributed to increased entrainment and upwelling on the right side of the hurricane's track (Chang and Anthes 1978, Price 1981, Son et al. 2006, Shi and Wang 2007). Resonance between the rotation of the hurricane's right-side wind stress vector and the ocean's inertial oscillations leads to more entrainment of cooler nutrient-rich water on the right than on the left; consequently, the increased nutrient flux causes a large bloom to form on the right (Chang and Anthes 1978, Price 1981, Subrahmanyam et al. 2002, Babin et al. 2004). However, a recent study by Huang and Oey (2015) concluded that vertical mixing alone can only produce a weak bloom

asymmetry. By examining the differences between 1-D and 3-D model experiments, they concluded that a subsurface jet created by the cyclone's asymmetric mixing caused submesoscale recirculation cells to form on the right side; these cells restratified the water in the euphotic zone, and produced bloom asymmetry comparable to that seen in nature.

Hurricanes can also produce asymmetric cooling and phytoplankton blooms on a continental slope and shelf (Tsuchiya et al. 2013, Allahdadi and Li 2017). As a hurricane moves closer to the continental slope and shelf, the ocean becomes well-mixed, and the response changes from baroclinic in the open ocean to barotrophic in shallow water less than 100 meters depth (Cooper and Thompson 1989a, Mitchell et al. 2005). Strong horizontal and vertical advection are associated with the hurricane's passing (Mitchell et al. 2005, Allahdadi and Li 2017), and they are important mechanisms of temperature change (Mitchell et al. 2005, Sheng et al. 2006). More recently, major hurricanes Harvey, Irma, and Maria (August and September 2017) devastated the coastal United States and Caribbean, causing at least 169 deaths and between $303 billion and $535 billion in damages as they moved from the deep ocean into the shallow shelf sea and onto the coast (BBC Business 2017, Rabin 2017, George et al. 2017, Friedman 2017, Rice 2017, Lee 2017, Pascual 2017, The Associated Press 2017). Despite the danger of these systems, their relative impacts on the ocean have not been thoroughly examined and compared. To fully understand the impacts of major storms, the change in ocean response due to changes in bathymetry must be considered.

The goal of this study is to further explore and understand the mechanisms behind asymmetric hurricane-induced cooling and phytoplankton blooms and compare and contrast

their responses in the deep open ocean and shallow shelf seas. To achieve that, an idealized model simulation and analysis approach is utilized.

2. METHODS AND DATA

2.1 Coupled Model Design

This study utilizes the Regional Ocean Modeling System (ROMS) coupled to a biological model described in Powell et al. (2006). ROMS is an advanced hydrostatic primitive-equation ocean model that computes values along a horizontal curvilinear Arakawa C grid and along vertically stretched terrain-following coordinates (Haidvogel et al. 2008, Powell et al. 2006, Warner et al. 2010, Zambon 2008). It uses the Boussinesq approximation and a time-stepping scheme that computes surface elevation and barotrophic momentum with short time steps, and uses longer steps for the equations of state (temperature, salinity, etc.) (Haidvogel et al. 2008). The Generic Length Scale (GLS) vertical mixing scheme (Umlauf and Burchard 2003, Warner et al. 2005a), with the Kantha and Clayson stability function (Kantha and Clayson 1994) is applied.

The idealized hurricane in this study is generated using the Holland wind model (Holland 1980). The wind profile for this model is

$$V_g = \left[\frac{AB(p_n - p_c)\, exp(-Ar^B)}{\rho r^B} + \frac{r^2 f^2}{4}\right]^{\frac{1}{2}} - \frac{rf}{2} \quad (1)$$

where V_g is the gradient wind at radius r, p_n is the ambient pressure, p_c is the central pressure, f is the Coriolis parameter, ρ is the air density, and A and B are constants. The differences due to central and ambient pressures have been removed by the parameter

$$\frac{p - p_c}{p_n - p_c} \tag{2}$$

which relates to *A* and *B* by the equation

$$A = r^B ln\left[\frac{p_n - p_c}{p - p_c}\right]. \tag{3}$$

The winds at the center are given by the equation

$$V_c = \left[\frac{AB(p_n - p_c)exp\left(-\frac{A}{r^B}\right)}{\rho r^B}\right]^{\frac{1}{2}} \tag{4}$$

where the radius of maximum wind can be found by taking the derivative of the equation above with respect to radius, and then setting the derivative equal to zero. This gives a radius of maximum winds that is independent of ambient and central pressure, or

$$R_w = A^{\frac{1}{B}} \tag{5}$$

which gives a maximum wind speed of

$$V_m = C(p_n - p_c)^{\frac{1}{2}} \tag{6}$$

where

$$C = \left(\frac{B}{\rho e}\right)^{\frac{1}{2}}. \tag{7}$$

In this model, instead of giving values to *A* and *B* directly, the values of the radius of maximum wind, the pressure in the hurricane's center, and the ambient pressure have been set. The ambient pressure is 1005 hPa, the hurricane's center pressure is 920 hPa, and the radius of maximum winds is 50 km.

Given the surface wind field produced by the Holland wind model, the wind stress scheme used in Oey et al. (2006) was subsequently used to calculate the wind stress needed by

the ocean model. In this scheme, a drag coefficient is calculated based on the magnitude of the wind speed. The drag coefficient is formulated so that at very high wind speeds, the magnitude of the drag coefficient levels off. The equations to calculate the drag coefficient are

$$C_d x10^3 = 1.2, W \leq 11\ m\ s^{-1} \tag{8}$$

$$C_d x10^3 = 0.49 + 0.065W, 11 < W \leq 19\ m\ s^{-1}$$

$$C_d x10^3 = 1.364 + 0.0234W - 0.0002W^2, 19 < W \leq\ 100\ m\ s^{-1},$$

where W is the wind speed in meters per second (Powell et al. 2003, Oey et al. 2006). Then, wind stress is calculated as

$$Stress = \ \rho C_d W^2. \tag{9}$$

A biological model described in Powell et al. (2006) was used to model the changes in nitrate and phytoplankton induced by the cyclone. This trophic model calculates dissolved nitrogen (nitrate, N), particulate nitrogen or detritus (D), phytoplankton (P), and zooplankton (Z) (see **Fig. 1**). The model calculates the amount of nitrogen contained within each group (in millimoles of nitrogen per meters cubed). The equations and parameters in this model are identical to those found in Spitz et al. 2003 (**Table 1**).

The dynamical equations (shown below) have the following form: the left side contains a local time derivative and an advection term, while the right contains a vertical mixing term plus the biological mechanisms. These mechanisms include grazing on phytoplankton by zooplankton (G), nitrogen uptake by phytoplankton (U), plankton removal (σ_d and ς_d, for phytoplankton and zooplankton respectively), sinking (w_d) and remineralization (δ).

$$\frac{\partial N}{\partial t} + \boldsymbol{u} \cdot \nabla N = \delta D + \gamma_n GZ - UP + \frac{\partial}{\partial z}\left(k_v \frac{\partial N}{\partial z}\right) \tag{10}$$

$$\frac{\partial P}{\partial t} + \boldsymbol{u} \cdot \nabla P = UP - GZ - \sigma_d P + \frac{\partial}{\partial z}\left(k_v \frac{\partial P}{\partial z}\right)$$

$$\frac{\partial Z}{\partial t} + \boldsymbol{u} \cdot \nabla Z = (1 - \gamma_n)GZ - \zeta_d Z + \frac{\partial}{\partial z}\left(k_v \frac{\partial Z}{\partial t}\right)$$

$$\frac{\partial D}{\partial t} + \boldsymbol{u} \cdot \nabla D = \sigma_d P + \zeta_d Z - \delta D + w_d \frac{\partial D}{dz} + \frac{\partial}{\partial z}\left(k_v \frac{\partial D}{\partial z}\right)$$

$$G = R_m(1 - e^{-\Lambda P})$$

$$I = I_0 \exp(k_z z + k_p \int_0^z P(z')dz'$$

$$U = \frac{V_m N}{k_N + N} \frac{\alpha I}{\sqrt{V_m^2 + \alpha^2 I^2}}.$$

Above, R_m is the zooplankton grazing rate, Λ is the Ivlev constant, I is the intensity of light, I_0 is the surface irradiance, k_z is the light extinction coefficient, k_p is the self-shading coefficient, V_m is the nitrate uptake rate, k_N is the uptake half saturation number, and α is the initial slope of the photosynthesis-irradiance curve.

In the original model, the amount of light at the ocean's surface remains constant with time, but for this study, a simple day-night cycle has been added, following that of Huang and Oey (2015). Solar irradiance is based on the typical amount of light in July in the subtropical region, and modeled with the following equation:

$$E_s = -533\, cos(\frac{2\pi t}{24}), E_s > 0 \qquad (11)$$

$$E_s = 0, E_s < 0$$

where t is time in hours. Unlike Huang and Oey (2015), the effects of cloud cover have not been considered.

2.2 Model Configuration

The domain is an idealized Cartesian basin with dimensions of 3600 km by 2800 km. The grid size is 8 km, and the basin has closed boundary conditions on the western boundary and gradient boundary conditions on all others. There are sixty-one vertical levels. **Fig. 2** shows the domain and the location of the hurricane's center at the beginning of each day. The Coriolis force has been approximated using a f-plane to simulate 15°N. Both deep ocean (Case 1) and continental shelf sea (Case 2) environments are considered. Case 1 has a constant bathymetry of 2000 m, whereas Case 2's bathymetry changes from 2000 m to 50 m over the slope and shelf (**Fig. 3**).

The hurricane wind forcing from the Holland model is one-way from the atmosphere to the ocean, neglecting air-sea interaction. As in Huang and Oey (2015), it moves in the east-west direction. The cyclone's initial position is at x = 3000 km, y = 1500 km. The hurricane's wind stress starts at zero and ramps up to its final strength over the course of twenty-four hours. This ramp-up was included to reduce numerical shock that can occur from a strong hurricane being introduced immediately into a still system. The hurricane translates from east to west at a constant speed of 5.5 m s^{-1}, and the simulation runs for a total of ten days.

Initial conditions for phytoplankton, nitrogen, and temperature at depth have been modeled in the manner of Huang and Oey (2015). Temperature is a function of depth, and is modeled by the set of equations:

$$T = 28.88°C \; for \; 0 < z < -30m, \tag{12}$$

$$T = 28.88 + [(28.88 - 8.5)\, tanh[\frac{z + 30}{175.9}]] \; for - 30m < z < -500m,$$

$$T = -3552.5z^{-0.967} \; for - 500m > z.$$

Nitrate is modeled by the set of equations:

$$NO3 = 0.05 \; for \; T \geq 26.8°C, \tag{13}$$

$$NO3 = -1.3458T + 36.094.$$

Nitrate is a function of temperature, also fitted using WOA data (Huang and Oey 2015). The initial phytoplankton profile is a shifted Gaussian function (Platt and Sathyendranath 1988, Sathyendranath et al. 1995, Huang and Oey 2015), such that phytoplankton concentrations are zero at approximately 200 m depth, with a value of 0.12 mmol N m^{-3} at the surface and a maximum of 0.37 mmol N m^{-3} at approximately 60 m depth. While Huang and Oey (2015) determined their chlorophyll *a* (chl *a*) profile in mg m^{-3}, for the purposes of this study, one mmol N m^{-3} is taken to be equal to 1 mg m^{-3} of chl *a* (Wroblewski 1989, Marra et al. 1990, Doney et al. 1995). **Fig. 4a** shows the initial vertical temperature and nitrate profiles, while **Fig. 4b** shows the initial zooplankton, phytoplankton, and detritus vertical profiles. Zooplankton and detritus values are set at a fixed value depending on the equivalent phytoplankton concentration at depth. Zooplankton concentration is equal to one-tenth the phytoplankton concentration, and detritus values are equal to twice the phytoplankton concentration. These proportions have been chosen after examining the output from the Southwest Atlantic Bight and Gulf of Mexico (SABGOM) model from the middle of the Gulf of Mexico over the water column (Hyun and He 2010, Xue et al. 2016).

3. RESULTS

3.1 Case 1

The ocean response to the hurricane is examined at both the surface and subsurface. For the surface analysis, a cross-section (xy-plane) is taken at Station B in **Fig. 2** and plotted over different inertial periods. One inertial period is 46.36 hours at 15^{o} N. The subsurface analysis is presented in a yz-cross-section, and the results have been zonally averaged over the black box shown in **Fig. 2** and then time-averaged over three inertial periods. The subsurface plots face westward, in the direction of hurricane motion. Thus the surface plots show evolution over time, while the subsurface plots are zonally- and time-averaged to show the overall lasting trends.

Noticeable surface cooling is observed along the track of hurricane (**Fig. 5**). The greatest SST decrease, -7°C, occurs on the right side of the hurricane's track (**Fig. 5a**). The surface current, showing a clear inertial oscillation pattern, is also several times greater on the right side of the track (**Fig. 5b**). As in Chang and Anthes (1978) and Price (1981), this asymmetric SST and mixed layer response occurs even with symmetric hurricane winds. The wind stress vector turns clockwise with time on the right, in the same direction as the ocean's inertial oscillations (Price 1981). This results in a resonance effect, which will be discussed further in Section 4.

The two areas of highest bloom concentration are not symmetric around the hurricane's center (**Fig. 6a**). One forms 40 km to the left of the center, and one nearly 160 km to the right of the center. At depths of 50 to 100 m, there is lower phytoplankton concentration on the right side than on the left. Temperature and nitrate contours are shifted to the right of the track such

that the greatest nitrate concentration occurs inside the area of greatest cooling, 10-120 km to the right of the hurricane's center. Upwelling, which is slightly shifted right, occurs up to 50 m depth, and is marked by areas of raised isotherms and low phytoplankton concentration.

The asymmetry in bloom position is correlated with the asymmetry in ocean mixing (**Fig. 6b**), represented by the log of the vertical diffusion coefficient (Kt). The wind mixing at the surface causes high Kt that penetrates down into the water column. At the surface, Kt is relatively higher on the left than on the right. However, the mixing extends to nearly 200 m depth on the right, compared to only 100 m on the left. Areas of relatively higher Kt are correlated with areas of relatively lower phytoplankton concentration, and vice versa.

The surface and subsurface asymmetry in phytoplankton concentrations can be described by mesoscale processes. The resonance between the turning of the wind stress vector and inertial oscillations causes more energy to enter the ocean on the right side than the left. Entrainment is increased on the right, which brings the existing subsurface chl *a* maximum, originally at 60 m depth, to the surface and brings cooler, chl *a*-poor water up to the mid-water column, contributing to both surface and subsurface asymmetry.

Recirculation cells, indicated by the alternating patterns of upward and downward momentum, occur on both the left and right sides of the track (**Fig. 7**). The cells on the right are stronger and extend deeper into the water column, moving water nearly eight meters per day. The area where the recirculation cells are the strongest coincides with the presence of a westward subsurface jet, indicated by the negative u values ($u = -0.4$ m s^{-1}) from 70 to 170 m depth and about 50 km to the right of the hurricane center. At the same time, an eastward surface jet of equivalent strength forms on the left side. The stronger recirculation cells on the

right re-stratify the top of the water column, and the decreased turbulence allows phytoplankton to bloom (Huisman et al. 1999). In this way, recirculation cells can be thought of as a "biological" mechanism of bloom asymmetry, as they promote new production primarily on the right side.

3.2 Case 2

There are two locations of interest in this experiment. The first is a cross-section that lies on the continental slope, where the depth is 200 m (Transect 1). The second is the shelf, where the bathymetry first reaches 50 m (Transect 2). The locations of these cross-sections are shown in **Fig. 2**. The slope location's results are considered first.

Asymmetry at the surface and subsurface increases on the slope relative to the deep ocean. There is a greater surface spreading of decreased SST, and the area of greatest cooling has shifted further to the right (**Fig. 8a**). Compared to the open ocean Case I, the inertially oscillating surface current is still greater on the right side of the track (**Fig. 8b**), though to a lesser extent.

The highest concentrations of phytoplankton and nitrate have shifted rightward as well, along with the area of greatest temperature decrease (**Fig. 8c**). At the subsurface, the phytoplankton concentrations on the left are higher than those on the right. There is a significant difference between the slope's Kt (**Fig. 8d**) and that of Case 1: on the right side of the track, Kt is high all the way to the ocean floor. This indicates that the surface mixed layer is starting to interact with the bottom boundary layer, and the ocean is moving to a well-mixed

condition. On the left side, the surface layer and bottom boundary layers are still separate enough to cause a subsurface asymmetry in Kt, keeping Kt relatively low.

The westward subsurface jet (u = -0.4 m s^{-1}) still forms on the right of the track (**Fig. 8e**), and there is an equally strong eastward surface jet on the left. Instead of clearly defined recirculation cells, water around the westward jet is moving upward from depths of 140 m, with speeds of greater than 26 m day^{-1}. A region of downwards motion has formed near the ocean floor on the right side of the track, accompanied by eastward subsurface motion (u = 0.2 m s^{-1}). This motion indicates that water near the slope's floor is moving off the slope and back into the open ocean. Aside from one region of upward motion on the left side, 60 km away from the hurricane's center, the water on the left side of the track moves downward off the slope.

The surface ocean's response at the shelf is even more asymmetric. **Fig. 9a** shows the change in SST at the shelf, which has a very strong rightward asymmetry. The inertially oscillating surface current quickly dissipates, due to a larger bottom friction effect in the shallow water (**Fig. 9b)**. The rightward shift in phytoplankton concentration, temperature, and nitrate is extreme, to the point where each variable is largely concentrated on the right side of the track (**Fig. 9c**). The water is shallow enough that it is well mixed and there is no difference in surface and subsurface asymmetry of phytoplankton. The well-mixed condition also inhibits formation of recirculation cells (**Fig. 9d**). The vertical momentum plot confirms that no recirculation cells occur (**Fig. 9e**). A weaker westward subsurface jet (u = -0.2 m s^{-1}) still develops on the right, while a stronger eastward surface jet (u = 0.4 m s^{-1}) forms on the left.

4. DISCUSSION

4.1 Inertial Oscillations

To understand the asymmetric mixing in Case 1, we examine the ocean's response to wind stress on the right and left sides of the hurricane's track. A hurricane's winds rotate counterclockwise in the Northern Hemisphere. As the hurricane moves forward through time, each point on the right side of the track feels the wind stress vector rotating clockwise with time, while each point on the left side feels the wind stress vector rotating counterclockwise with time (Price 1981, Chang and Anthes 1978). The inertial oscillations induced in the ocean by the wind stress have the form

$$\frac{du}{dt} - fv = 0 \qquad (14)$$
$$\frac{dv}{dt} + fu = 0,$$

and due to the influence of the Coriolis effect, turn to the right on both sides of the hurricane's track. Since both the inertial oscillations and the wind stress vector are turning in the same direction on the right, the water on the right is accelerated more than that on the left (Price 1981, Chang and Anthes 1978). This induces mixing deeper into the water column on the right side than the left.

Inertial oscillations usually propagate from areas with larger *f* to areas with smaller *f*, but relative vorticity can shift *f* to an effective Coriolis parameter (f_{eff}), allowing some waves to propagate freely and others to be trapped and amplified (Anderson and Gill 1979, Kunze 1985, Oey et al. 2008, Qian et al. (in review)). The effective Coriolis parameter is calculated as

$$f_{eff} = f + \frac{\zeta}{2} \quad (15)$$

where ζ is the vertical component of relative vorticity (RV). Near-inertial waves become trapped in regions of negative vorticity, where f_{eff} is lower than the f of the surrounding ocean, while regions of positive vorticity increase f_{eff} and dampen the propagation of near-inertial waves (Kunze 1985, Qian et al. in review). **Fig. 10** shows ζ normalized by f, averaged zonally and over three inertial periods. The asymmetric RV response may provide insights into how the inertial energy propagates. On the right, RV/f values are uniformly low to depths of 200 meters, and the decrease in f_{eff} as it moves away from the hurricane center allows inertial waves and their energy to propagate vertically deep into the water column. On the left, the maximum positive RV/f occurs within the radius of maximum winds (50 km), which increases f_{eff} relative to the ocean around it and dampens inertial oscillations. An area of lowest (negative) RV/f occurs at nearly 100 km to the left of the cyclone. It is surface trapped, and corresponds to an area of high Kt. Inertial oscillations are generated and are propagating downward in the negative RV area, more so on the right than the left. Once the right-side inertial oscillations can no longer propagate vertically, the remaining energy is channeled into the subsurface jet (Kunze 1985, Oey et al. 2008, Huang and Oey 2015).

4.2 Recirculation Cells and PV Dynamics

As discussed earlier, the surface and subsurface jets are associated with the formation of recirculation cells. While the cells form on both sides of the track, they are stronger and deeper on the right. The recirculation cells re-stratify the top of the water column. The development of recirculation cells can be elucidated in the context of potential vorticity (PV).

Thomas (2005) examines conditions in which PV is destroyed by defining the PV "q" equation and its rate of change as

$$q = f\omega_a \cdot \nabla b; \quad \frac{dq}{dt} = -\nabla \cdot J = -\nabla \cdot (qu + f\nabla b \times F - fD\omega_a); \tag{16}$$

where $\omega_a = fk + \nabla \times u$ is the absolute vorticity, f is the Coriolis parameter, k is the vertical unit vector, u is velocity, $b=-g\rho/\rho_o$ is the buoyancy, g is the gravitational acceleration, ρ is the density, ρ_o is a reference density, qu is an advective constituent, F represents frictional forces, and D represents diabatic processes. Since there is no air-sea coupling in this study, only the frictional forces will be considered. Thomas (2005) integrated dq/dt over a control volume bounded by isopycnal surfaces and an upper surface open to the air-sea interface, and found that dq/dt was a function of the surface PV flux associated with frictional forces (J_z^F), expressed as

$$J_z^F = f\nabla_h b \times F. \tag{17}$$

For PV to be destroyed, a situation in which dq/dt < 0 (or J > 0), the wind stress should be perpendicular to the horizontal density gradient, which is outward from the cooler upwelled water at the storm's center (Thomas 2005, Huang and Oey 2015).

In Case 1 for example, there is indeed buoyancy loss due to wind mixing at the surface layer, and density gradients that vary laterally throughout the mixed layer. In its simplest (2D) form, this situation causes convection cells to develop which slant sideways due to the thermal wind balance between the lateral density gradient and a meridional current (Haine and Marshall 1998). The fluid particles move along these slantwise paths in a process called symmetric instability. If PV is negative, then these cells are unstable and the motion of the water will return PV to zero, re-stratifying the water column (Haine and Marshall 1998). **Fig. 11(a, b, c)**

shows the initial zonally-averaged relative vorticity (RV), buoyancy (calculated as b = $-g(\rho-\rho_o)/\rho_o$), and PV($= -(\frac{f}{\rho})(\partial\rho/\partial z)$= -(f/g)$N^2$) at day 0; **Fig. 11(d, e, f)** shows the zonally-averaged and time-averaged (between day 1 and day 6.8, three inertial periods) RV, buoyancy, and PV; and **Fig. 11(g, h, i)** shows the change over time between the averaged plots and the initial plots. The averaged buoyancy reveals a frontal zone, caused by the upwelled cooler water near the hurricane's center. The surface buoyancy is lower at the hurricane's center and gradually increases outward from the center, producing a positive outward horizontal density gradient. Between 0 and 25 m depth, PV decreases over time by up to 0.015 m^{-1} s^{-1}. This indicates that the surface PV flux (J) in this region is positive, change in PV is negative, and that there is PV destruction and restratification occurring in this region. Indeed, **Fig. 12** shows the time-averaged change in surface PV (dq/dt) over the black box in **Fig. 2**. Regions of PV loss occur on both the right and left sides of the track. The horizontal buoyancy gradient is radially outward from the center on both sides, and the direction of wind stress (westward on the right, eastward on the left) on either side gives a positive curl, leading to PV destruction. The region of positive dq/dt at the eastern boundary may be a combination of model numerical shock from the introduction of the hurricane and the clockwise turning of the wind-stress vector over time, which would cause wind stress on the right to move in an easterly direction, leading to negative curl and increased dq/dt.

In Case 2, strong recirculation cells do not form (**Fig. 9e**). The interaction of the surface and bottom boundary layers and the resulting well-mixed ocean (**Fig. 9d**) inhibits the formation of recirculation cells.

5. CONCLUSION

This research sought to determine the mechanisms that produced asymmetric phytoplankton blooms in the wake of hurricanes in the Northern Hemisphere. It used an idealized coupled physical-biological ocean model forced by the symmetric Holland wind fields. Both a constant depth open ocean case (Case 1) and a shelf sea case (Case 2) were considered.

A conceptual model (**Fig. 13)** was proposed that combined mesoscale and submesoscale processes to give a broad view of what causes bloom asymmetry in the ocean. As the hurricane moves along its track, it induces entrainment that mixes the existing subsurface chl *a* maximum into the surface. Since more water is entrained on the right side than the left, more chl *a* and nutrients are mixed into the surface on the right. After the hurricane has passed, the horizontal density gradient and upward flux of potential vorticity cause the formation of recirculation cells that destroy potential vorticity and restratify the surface layer, creating a more favorable condition for phytoplankton to bloom. While recirculation cells do appear on both sides of the hurricane's track, they are more prominent on the right side, where the greater density gradient occurs. A subsurface jet in the direction of hurricane motion also develops on the right in conjunction with these recirculation cells.

The mechanisms behind right-side bloom asymmetry on the shelf are very different from the open ocean case, as indicated by **Fig. 13**. The strong wind mixing, in conjunction with the shallow water depth, causes the surface and bottom boundary layers to merge, which hinders the formation of inertial oscillations and recirculation cells. Instead, surface currents moving in the direction of the wind stress develop, moving onshore on the right and offshore

on the left. A downwelling condition develops on the right side on the slope. The convergence of water on the right causes a build-up of cooler water, nitrate, and phytoplankton on the right, while water on the left is transported offshore.

This conceptual model opens the door for more research on phytoplankton bloom asymmetry. One future area of research lies in understanding the effect that hurricane-induced phytoplankton blooms have on the ocean's carbon cycle. The partial pressure of CO_2 in water (pCO_2w) is a function of primary production, gas exchange, alkalinity and dissolved inorganic carbon concentrations (DIC), which in turn are functions of ocean temperature and salinity (Bates et al. 1998a). Earlier studies have shown that hurricanes may increase, decrease, or cause little change in pCO_2w based on the region of the world ocean and the time of year (Mahadevan et al. 2011). Other studies have shown that in general, hurricanes cause an efflux of CO_2 from the ocean to atmosphere, in contrast to the ocean's usual role as a carbon sink (Bates et al. 1998a, Nemoto et al. 2009, Koch et al. 2009, Huang and Imberger 2010, Bond et al. 2011). These studies however did not adequately consider the effects of biological production, which can be the primary driver of the carbon sink (Xue et al. 2016). By using this research's model configuration in conjunction with biogeochemical models that consider organic and inorganic carbon budgets (e.g. Fennel et al. 2006, 2008), the relative contribution of phytoplankton blooms to atmosphere-ocean carbon exchange can be better quantified.

Another area of future research is in the effect of ocean-atmosphere-wave interactions on phytoplankton bloom asymmetry. In this study, the ocean did not provide feedback to the atmosphere, nor were wave effects included. However, previous studies have shown that the feedback from the ocean to the atmosphere as a hurricane passes over cooler water decreases

hurricane intensity (Emanuel 1999, Gierach and Subrahmanyam 2008, Walker et al. 2014, Zambon et al. 2014), while the magnitude of the ocean's response depends on the intensity and translation speed of the hurricane (Chang and Anthes 1978, Price 1981). The addition of waves would create a greater surface roughness, increase ocean mixing, change wind stress, and cause wave-current interactions (Warner et al. 2010). Whether or not these considerations would change the framework of the conceptual model presented in this study needs to be examined and reported in a future study. The resulting understanding will shed light on important processes that are required for accurate coupled marine physical-biogeochemical prediction problems in a real world.

REFERENCES

Allahdadi MN, Chunyan L (2017) Numerical Simulation of Louisiana Shelf Circulation under Hurricane Katrina. Journal of Coastal Research. (In-Press)

Babin SM, Carton JA, Dickey TD, Wiggert JD (2004) Satellite evidence of hurricane-induced phytoplankton blooms in an oceanic desert. Journal of Geophysical Research: Oceans 109:C03043. doi: 10.1029/2003JC001938

Bates NR, Knap AH, Michaels AF (1998a) Contribution of hurricanes to local and global estimates of air-sea exchange of CO2. Nature 395:58-61. doi: 10.1038/25703

BBC Business (2017) Hurricane Irma: Florida assesses damage as storm weakens. BBC News. www.bbc.com/news/business-41231323. Accessed 1 October 2017

Bond NA, Cronin MF, Sabine C, et al (2011) Upper ocean response to Typhoon Choi-Wan as measured by the Kuroshio Extension Observatory mooring. Journal of Geophysical Research 116:C02031. doi: 10.1029/2010JC006548

Chang SW, Anthes RA (1978) Numerical Simulations of the Ocean's Nonlinear, Baroclinic Response to Translating hurricanes. Journal of Physical Oceanography 8(3):468-480.

Cooper C, Thompson JD (1989a) Hurricane-generated currents on the outer continental shelf. 1. Model formulation and verification. Journal of Geophysical Research: Oceans 94(C9): 12513-12539.

Doney SC, Glover DM, Najjar RG (1995) A new coupled, one-dimensional biological-physical model for the upper ocean: Applications to the JGOFS Bermuda Atlantic Time-series Study (BATS) site. Deep-Sea Research II 43(2-3):591-624.

Emanuel KA (1999) Thermodynamic control of hurricane intensity. Nature 401:665-669.

Fennel K, Wilkin J, Levin J, et al (2006) Nitrogen cycling in the Middle Atlantic Bight: Results from a three-dimensional model and implications for the North Atlantic nitrogen budget. Global Biogeochemical Cycles 20(3):GB3007. doi: 10.1029/2005GB002456

Fennel K, Wilkin J, Previdi M, Najjar R (2008) Denitrification effects on air-sea CO_2 flux in the coastal ocean: Simulations for the northwest North Atlantic. Geophysical Research Letters 35(24):L24608. doi: 10.1029/2008GL036147

Friedman N (2017) Hurricane Maria Caused as Much as $85 Billion in Insured Losses, AIR Worldwide Says. The Wall Street Journal. https://www.wsj.com/articles/hurricane-maria-caused-as-much-as-85-billion-in-insured-losses-air-worldwide-says-1506371305?. Accessed 1 October 2017

George C, Kadifa M, Ellis L, et al (2017) Storm deaths: Harvey claims lives of more than 75 in Texas. Houston Chronicle (chron.com). www.chron.com/news/houston-weather/hurricaneharvey/article/Harvey-Aftermath-Houston-police-officer-dies-19-12159139.php. Accessed 1 October 2017

Gierach MM, Subrahmanyam B (2008) Biophysical responses of the upper ocean to major Gulf of Mexico hurricanes in 2005. Journal of Geophysical Research 113:C04029. doi: 10.1029/2007JC004419

Haidvogel DB, Arango H, Budgell WP, et al (2008) Ocean Forecasting in Terrain-following Coordinates: Formulation and Skill Assessment of the Regional Ocean Modeling System. Journal of Computational Physics 227:3595-3624

Haine TN, Marshall J (1998) Gravitational, Symmetric, and Baroclinic Instability of the Ocean Mixed Layer. Journal of Physical Oceanography 28:634-658. doi: 10.1175/1520-0485(1998)020<0634:GSABIO>2.0.CO;2

Holland GJ (1980) An Analytic Model of the Wind and Pressure Profiles in Hurricanes. Monthly Weather Review 108:1212-1218.

Huang P, Imberger J (2010) Variation of pCO_2 in ocean surface water in response to the passage of a hurricane. Journal of Geophysical Research: Oceans 115:C10024. doi: 10.1029/2010JC006185

Huang S-M, Oey L-Y (2015) Right-side cooling and phytoplankton bloom in the wake of a tropical cyclone. Journal of Geophysical Research: Oceans 120:5735–5748. doi: 10.1002/2015JC010896

Huisman J, van Oostveen P, Weissing FJ (1999) Critical depth and critical turbulence: Two different mechanisms for the development of phytoplankton blooms. Limnology and Oceanography 44(7):1781-1787.

Hyun KH, He R (2010) Coastal upwelling in the South Atlantic Bight: A revisit of the 2003 cold event using long term observations and model hindcast solutions. Journal of Marine Systems 83:1-13.

Kantha LH, Clayson CA (1994) An improved mixed layer model for geophysical applications. Journal of Geophysical Research 99:25235-25266. doi: 10.1029/94JC02257

Koch J, McKinley GA, Bennington V, Ullman D (2009) Do hurricanes cause significant interannual variability in the air-sea CO_2 flux of the subtropical North Atlantic? Geophysical Research Letters 36:L07606. doi: 10.1029/2009GL037553

Kunze E (1985) Near-inertial wave propagation in geostrophic shear. Journal of Physical Oceanography 15:544-565.

Lee D (2017) Harvey is likely to be the second-most costly natural disaster in U.S. history. Los Angeles Times. www.latimes.com/business/la-fi-harvey-economic-toll-20170901-story.html. Accessed 1 October 2017

Mahadevan A, Tagliabue A, Bopp L, et al (2011) Impact of episodic vertical fluxes on sea surface pCO_2. Philosophical Transactions of the Royal Society A: Mathematical, Physical and Engineering Sciences 369:2009–2025. doi: 10.1098/rsta.2010.0340

Marra J, Bidigare RR, Dickey TD (1990) Nutrients and mixing, chlorophyll and phytoplankton growth. Deep-Sea Research 37:127-143.

Mitchell DA, Teague WJ, Jaroz E, Wang DW (2005) Observed currents over the outer continental shelf during Hurricane Ivan. Geophysical Research Letters. doi: 10.1029/2005GL023014

Nemoto K, Midorikawa T, Wada A, et al (2009) Continuous observations of atmospheric and oceanic CO2 using a moored buoy in the East China Sea: Variations during the passage of typhoons. Deep Sea Research Part II: Topical Studies in Oceanography 56:542–553. doi: 10.1016/j.dsr2.2008.12.015

Oey L-Y, Ezer T, Wang D-P, et al (2006) Loop Current warming by Hurricane Wilma. Geophysical Research Letters 35:L12604. doi: 10.1029/2006GL025873

Oey L-Y, Inoue M, Lai R, et al (2008) Stalling of near-inertial waves in a cyclone. Geophysical Research Letters 35:L12604. doi: 10.1029/2008GL034273

Pascual OS (2017) Hurricane Maria's death toll in Puerto Rico is higher than official count, experts say. Miami Herald. www.miamiherald.com/news/weather/hurricane/article175955031.html. Accessed 1 October 2017.

Platt T, Sathyendranath S (1988) Oceanic primary production: estimation by remote sensing at local and regional scales. Science 241(4873):1613-1620.

Powell MD, Vlckery PJ, Relnhold TA (2003) Reduced drag coefficient for high wind speeds in tropical cyclones. Nature 422:279-283.

Powell TM, Lewis CVW, Curchitser EN, et al (2006) Results from a three-dimensional, nested biological-physical model of the California Current System and comparisons with statistics from satellite imagery. Journal of Geophysical Research 11:C07018. doi: 10.1029/2004JC002506

Price JF (1981) Upper Ocean Response to a Hurricane. Journal of Physical Oceanography 11:153-175.

Qian H, Hamilton P, Sheinbaum J, et al (in review) Divergence of ocean inertial response to the passage of Hurricane Ida in the Gulf of Mexico. Journal of Physical Oceanography.

Rabin C (2017) Unofficial death toll from Hurricane Irma now stands at 75 across the state. Miami Herald. www.miamiherald.com/news/weather/hurricane/article175029276.html. Accessed 1 October 2017.

Rice D (2017) Harvey to be costliest natural disaster in U.S. history, estimated cost of $190 billion. USA Today. https://www.usatoday.com/story/weather/2017/08/30/harvey-costliest-natural-disaster-u-s-history-estimated-cost-160-billion/615708001/. Accessed 1 October 2017

Sathyendranath S, Longhurst A, Caverhill CM, et al (1995) Regionally and seasonally differentiated primary production in the North Atlantic. Deep Sea Research 42(10):1773-1802.

Sheng J, Zhai X, Greatbatch RJ (2006) Numerical study of the storm-induced circulation on the Scotian Shelf during Hurricane Juan using a nested-grid ocean model. Progress in Oceanography 70:233–254. doi: 10.1016/j.pocean.2005.07.007

Shi W, Wang M (2007) Observations of a Hurricane Katrina-induced phytoplankton bloom in the Gulf of Mexico. Geophysical Research Letters 34:611607. doi: 10.1029/2007GL029724

Son S, Platt T, Bouman H, et al (2006) Satellite observation of chlorophyll and nutrients increase induced by Typhoon Megi in the Japan/East Sea. Geophysical Research Letters 33:L05607. doi: 10.1029/2005GL025065

Subrahmanyam B, Rao KH, Srinivasa Rao N, et al (2002) Influence of a tropical cyclone on Chlorophyll-a Concentration in the Arabian Sea. Geophysical Research Letters 29(22):2065. doi: 10.1029/2002GL015892

The Associated Press (2017) Hurricane Maria death toll rises as storm kicks up ocean on the coast. Orlando Sentinel. www.orlandosentinel.com/weather/hurricane/os-hurricane-maria-dominica-death-toll-20170925-story.html. Access 1 October 2017.

Tsuchiya K, Yoshiki T, Nakajima R, et al (2013) Typhoon-driven variations in primary production and phytoplankton assemblages in Sagami Bay, Japan: A case study of typhoon *Mawar* (T0511). Plankton and Benthos Research 8(2):74-87.

Umlauf L, Burchard H (2003) A generic length-scale equation for geophysical turbulence models. Journal of Marine Research 61:235–265. doi: 10.1357/002224003322005087

Walker ND, Leben RR, Pilley CT, et al (2014) Slow translation speed causes rapid collapse of northeast Pacific Hurricane Kenneth over cold core eddy: Northeast Pacific Hurricane Collapses. Geophysical Research Letters 41:7595–7601. doi: 10.1002/2014GL061584

Warner JC, Armstrong B, He R, Zambon JB (2010) Development of a Coupled Ocean–Atmosphere–Wave–Sediment Transport (COAWST) Modeling System. Ocean Modeling 35:230–244. doi: 10.1016/j.ocemod.2010.07.010

Warner JC, Sherwood CR, Arango HG, et al (2005a) Performance of four turbulence closure methods implemented using a generic length scale method. Ocean Modeling 8:81-113.

Wroblewski JS (1989) A model of the spring bloom in the North Atlantic and its impact on ocean optics. Limnology and Oceanography 34(8):1563-1571.

Xue Z, He R, Fennel K, et al (2016) Modeling pCO_2 variability in the Gulf of Mexico. Biogeosciences 13:4359–4377. doi: 10.5194/bg-13-4359-2016

Zambon, JB (2008) An Examination of Tropical Cyclone Dynamics Utilizing the 3-Way Coupled Ocean Atmosphere Wave Sediment Transport (COAWST) Model. Master's thesis, North Carolina State University. http://www.lib.ncsu.edu/resolver/1840.16/475.

TABLES

Table 1. Parameters in the NPZD Powell biological model. Values are the same as those in Spitz et al. 2003 and Powell et al. 2006

Name	**Value**	**Dimension**
Light extinction coefficient (k_z)	0.067	m^{-1}
Self-shading coefficient (k_p)	0.0095	m^2 mmol N^{-1}
Initial slope of P-I curve (α)	0.025	m^2 W^{-1}
Nitrate uptake rate (V_m)	1.5	d^{-1}
Uptake half saturation (k_N)	1.0	mmol N m^{-3}
Phytoplankton senescence (σ_d)	0.1	d^{-1}
Zooplankton grazing rate (R_m)	0.52	d^{-1}
Ivlev constant (λ)	0.06	m^3 mmol N^{-1}
Excretion efficiency (γ_n)	0.3	
Zooplankton mortality (ζ_d)	0.145	d^{-1}
Remineralization (δ)	1.03	d^{-1}
Detrital sinking rate (w_d)	8.0	m d^{-1}

FIGURES

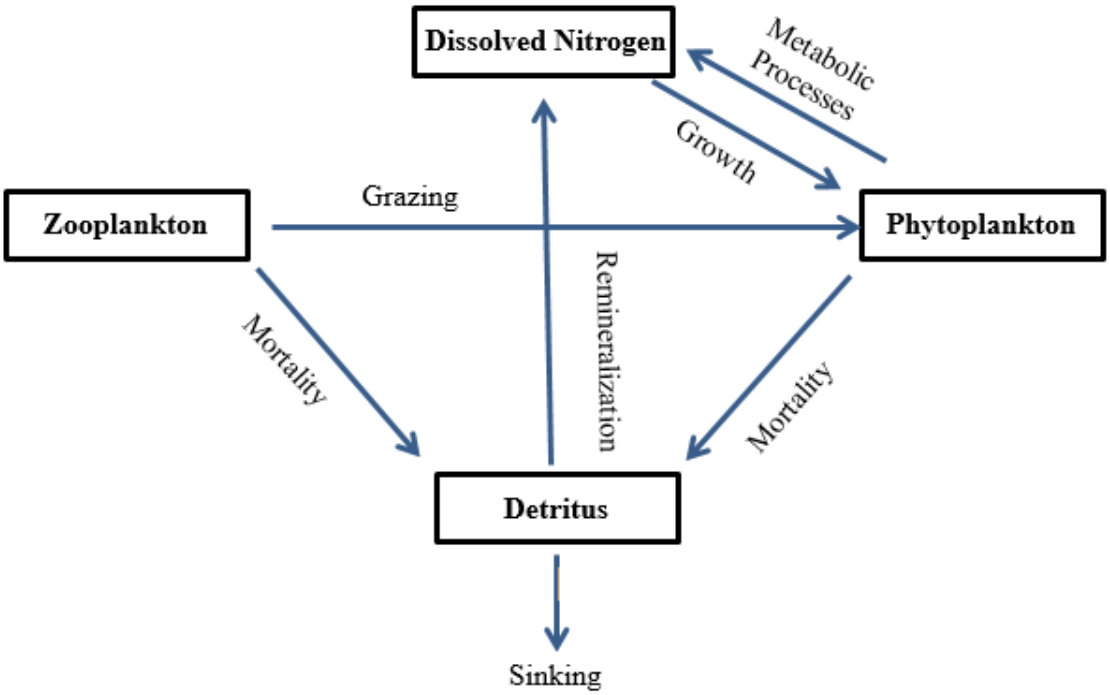

Fig. 1 A diagram of processes modeled by the Powell biological model. The model calculates variable concentrations in terms of nitrogen storage. Phytoplankton incorporate nitrate, grow, and go through senescence, becoming detritus. Zooplankton graze on phytoplankton, grow, and die, also contributing to the detrital pool. Detrital material is remineralized into dissolved nutrients (i.e., nitrate) or exported as it sinks

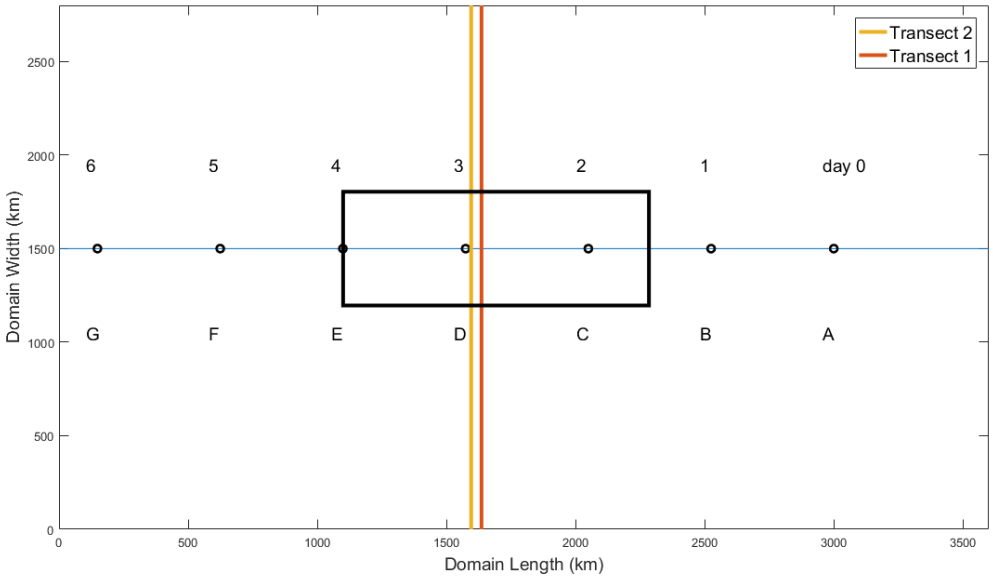

Fig. 2 The ROMS model domain, 3600 km by 2800 km. Black circles denote the location of the hurricane's center at the beginning of the day labeled above it; each circle has been given a station letter. The black box in the center is the zonally averaged area

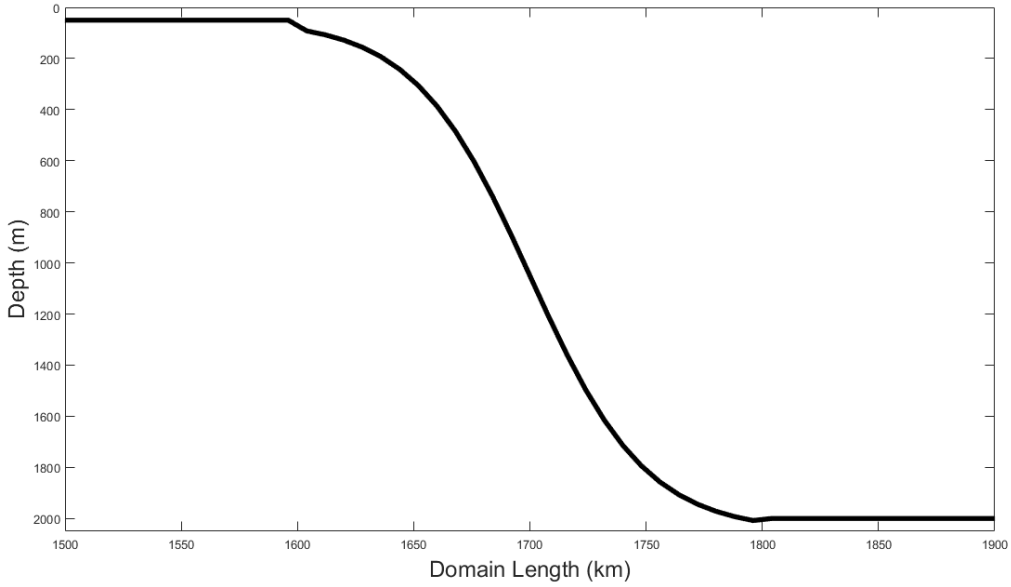

Fig. 3 Bathymetry in Case 2, which changes from 2000 m to 50 m over the length of the domain

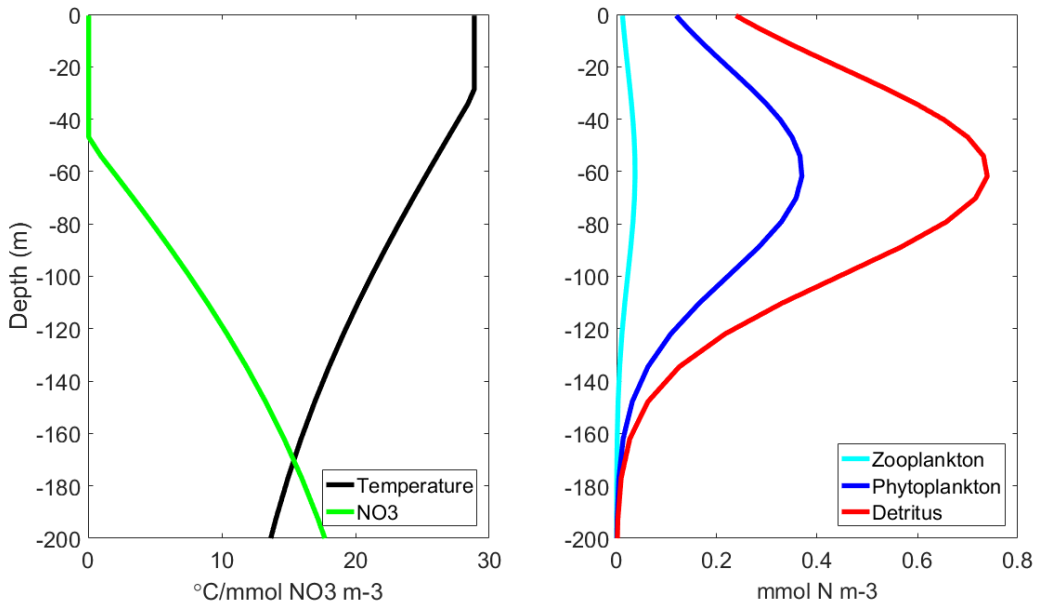

Fig. 4 (a) Initial profiles of temperature (°C, black) and nitrate (mmol NO_3 m^{-3}, green). (b) Initial profiles of zooplankton (cyan), phytoplankton (blue) and detritus (red), all in mmol N m^{-3}

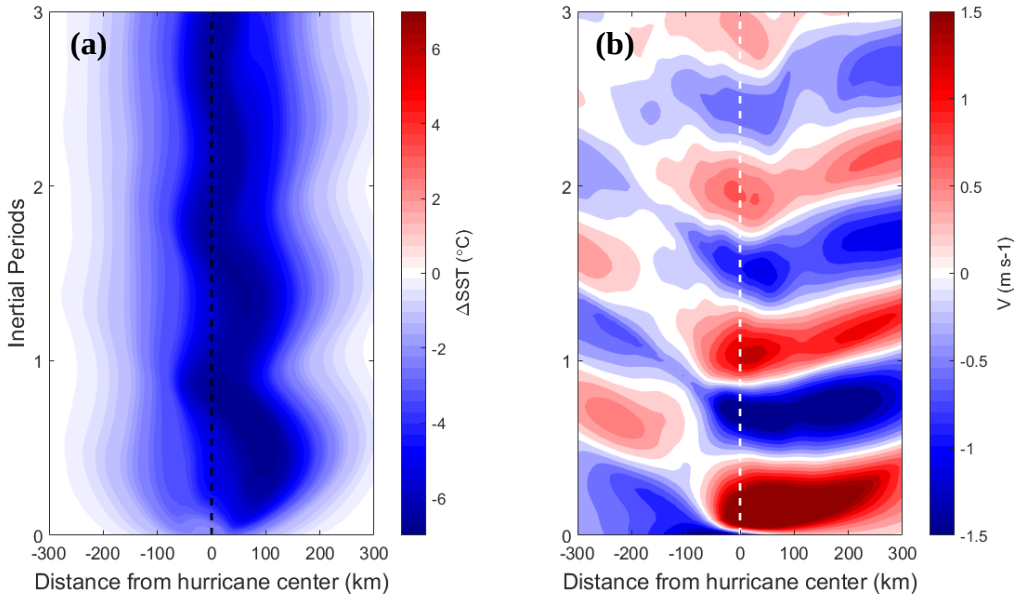

Fig. 5 (a) ΔSST (°C) at Station B over three inertial periods for Case 1. The black dashed line indicates the hurricane center. (b) Meridional velocity (m s^{-1}) at Station B over three inertial periods. The white dashed line indicates the hurricane center

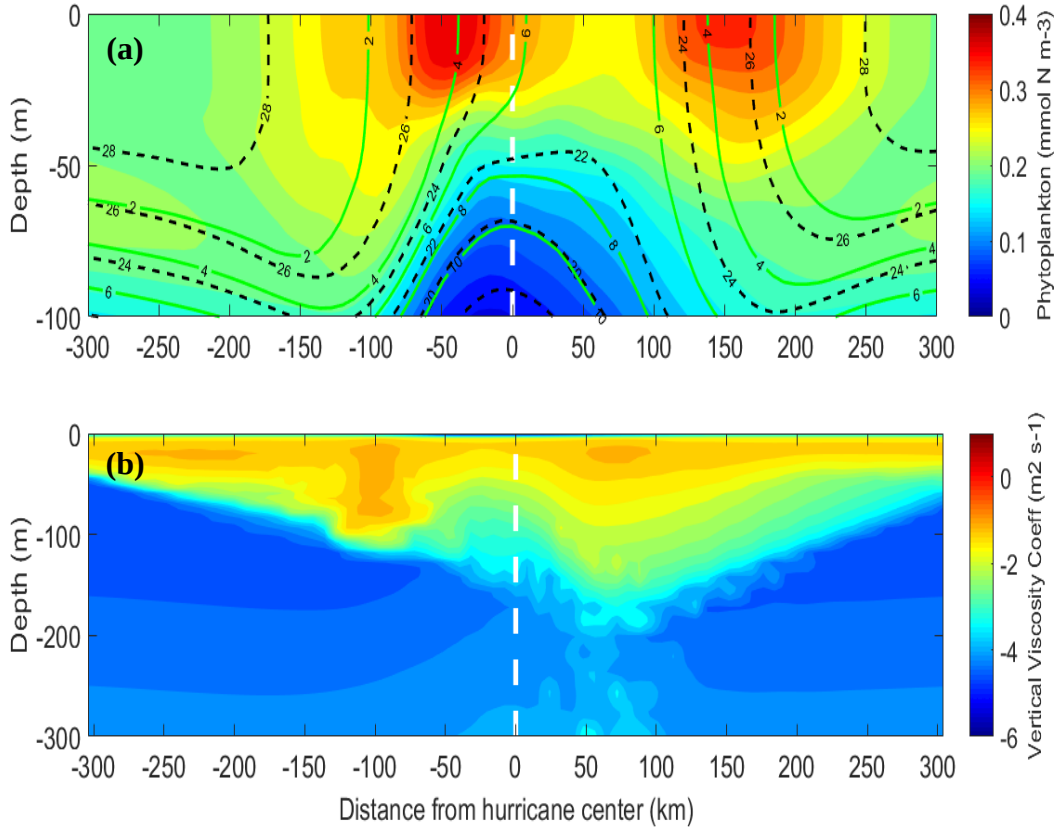

Fig. 6 (a) Time-averaged phytoplankton (shading), temperature (black dashed contours), and nitrate (green contours) in the yz-plane. (b) Time-averaged $\log_{10}$ of the vertical viscosity coefficient (Kt). The white dashed line indicates the hurricane center. The view is westward in the direction of the translating hurricane, and the variables have been zonally averaged over the box in Fig. 2 as well as time-averaged for three inertial periods

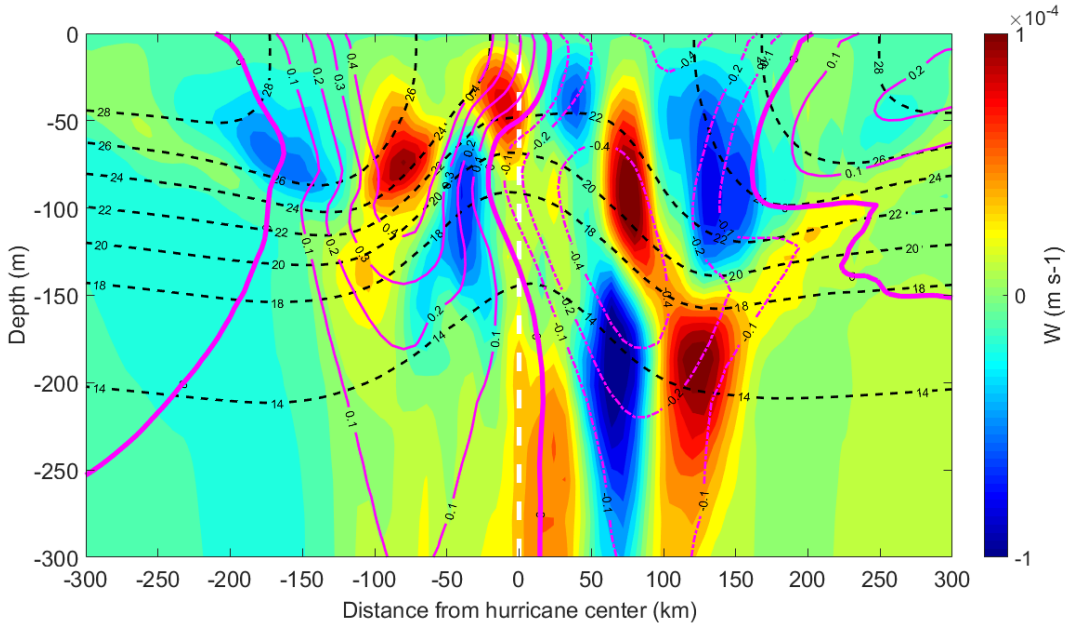

Fig. 7 Time-averaged vertical velocity (W in m s^{-1}, shading), temperature (black contours) and zonal velocity (m s^{-1}, magenta contours; dashed lines indicate westward motion, solid lines indicate eastward motion, and bold lines indicate zero motion) for Case 1. All variables have been zonally averaged over the box in Fig. 2 and time-averaged over three inertial periods. The view is westward in the direction of the translating hurricane, and the white dashed line indicates the hurricane center

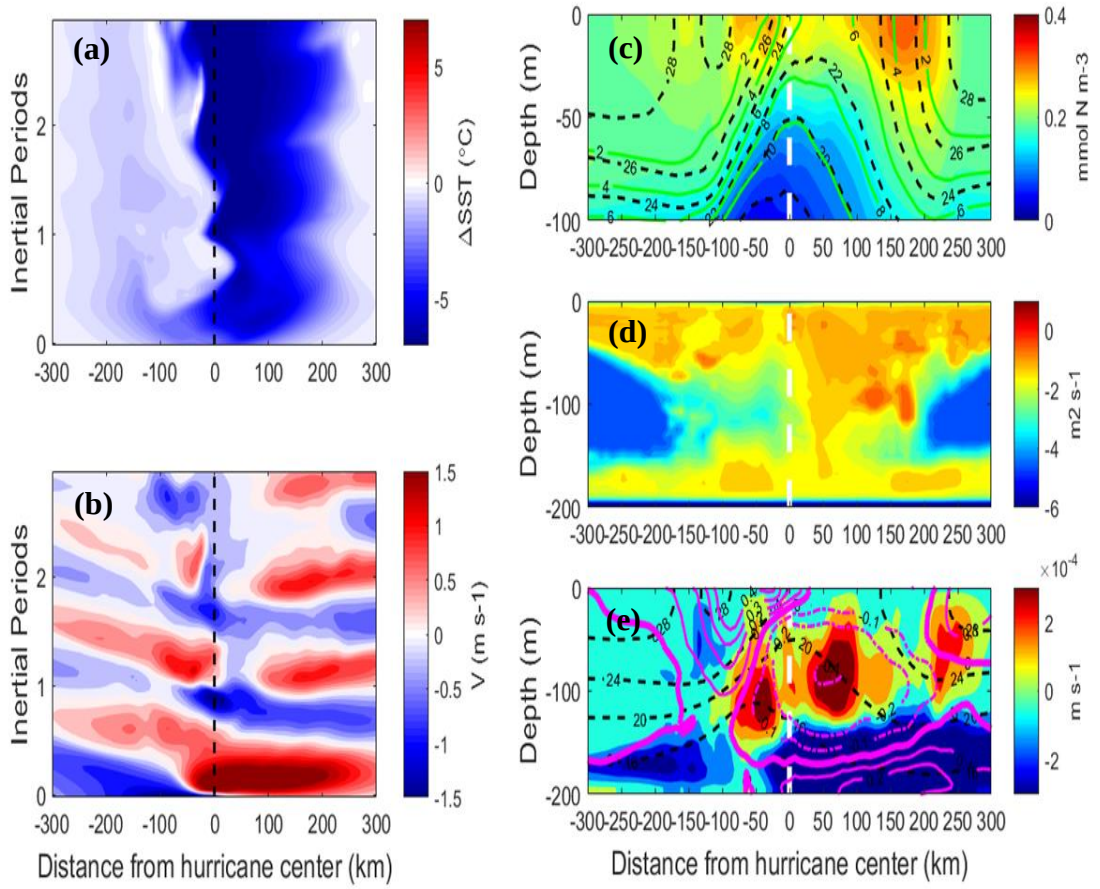

Fig. 8 Case 2: continental shelf sea, results at Transect 1. (a) ΔSST over three inertial periods for the slope (200 m depth). (b). Meridional velocity (V) over three inertial periods. (c) Time-averaged phytoplankton (shading), temperature (black contours, °C), and nitrate (green contours, mmol NO_3 m^{-3}). (d) Time-averaged $\log_{10}$ of the vertical viscosity coefficient (Kt). (e) Time-averaged vertical velocity (shading), temperature (black contours), and zonal velocity (magenta contours; dashed for westward motion, solid for eastward motion, bold for zero motion). White dashed lines indicate the hurricane center. The views are westward in the direction of the translating hurricane

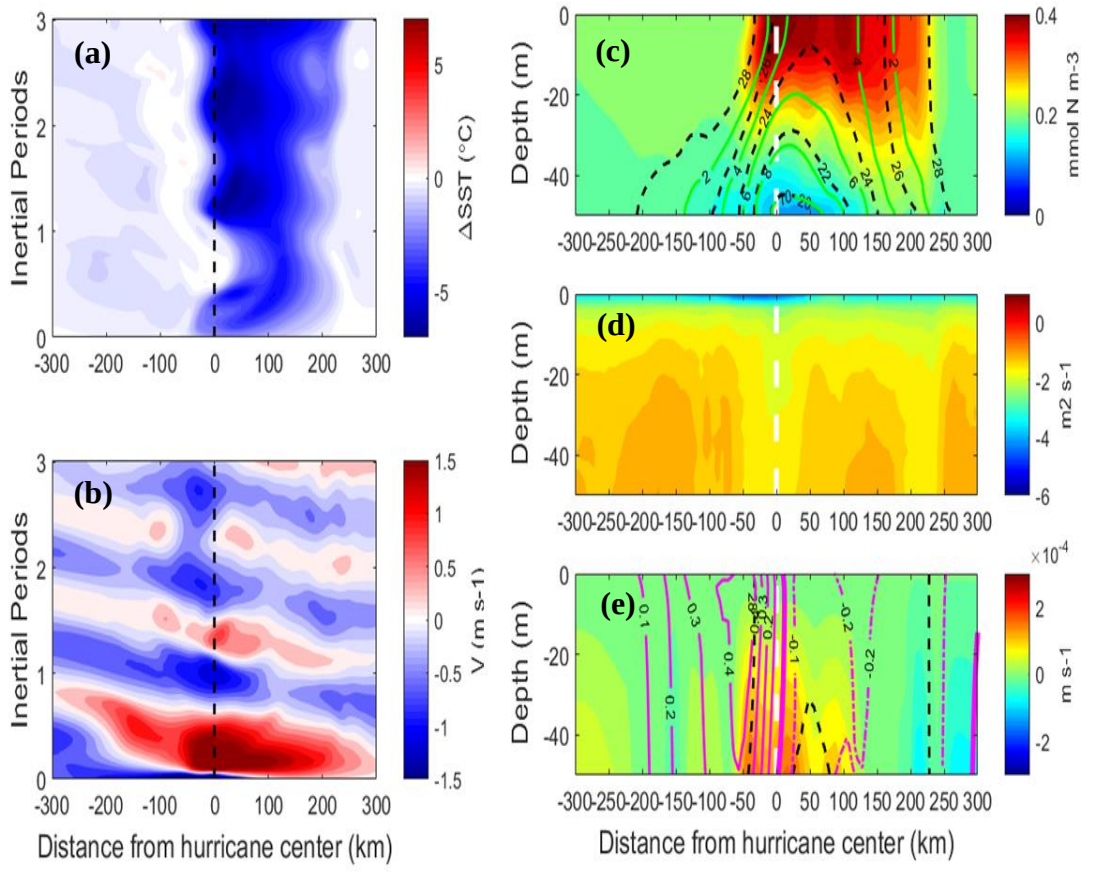

Fig. 9 Case 2: continental shelf sea, results at Transect 2. (a) ΔSST over three inertial periods. (b) Meridional velocity (m s^{-1}) over three inertial periods. (c) Time-averaged phytoplankton (shading), temperature (black contours, °C), and nitrate (green contours, mmol NO_3 m^{-3}). (d) Time-averaged $\log_{10}$ of the vertical viscosity coefficient (Kt). (e) Time-averaged vertical velocity (shading), temperature (black contours), and zonal velocity (magenta contours; dashed for westward motion, solid for eastward motion, bold for zero motion). White dashed lines indicate the hurricane center. The views are westward in the direction of the translating hurricane

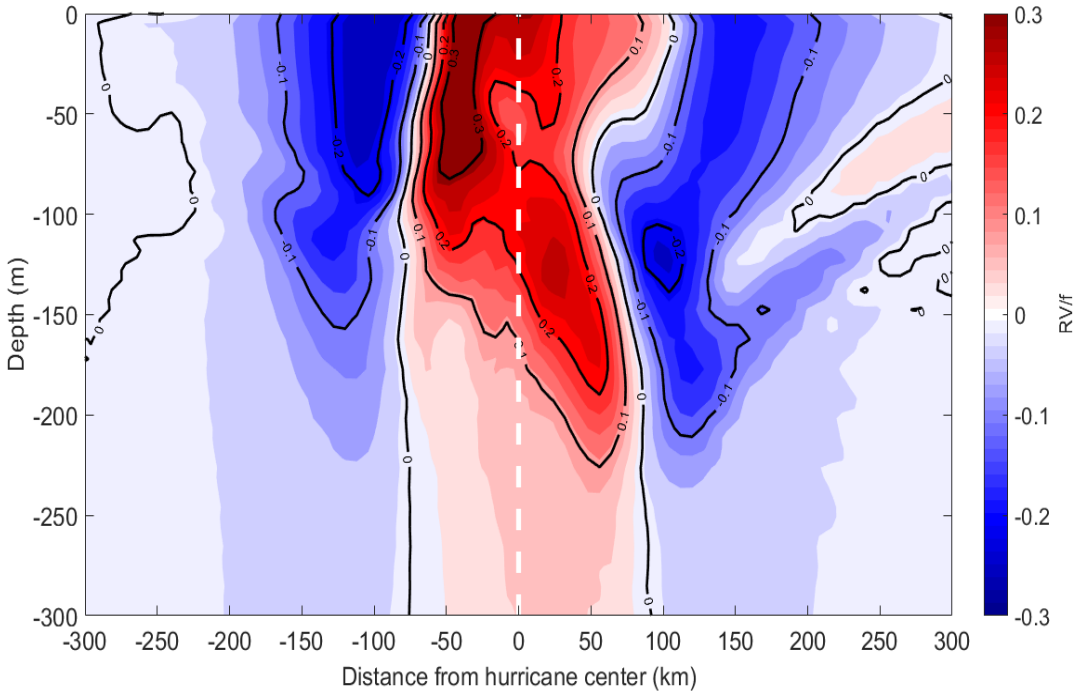

Fig. 10 Relative vorticity (RV), normalized by *f*, for Case 1. The variable has been averaged zonally and over three inertial periods. The view is westward in the direction of the translating hurricane

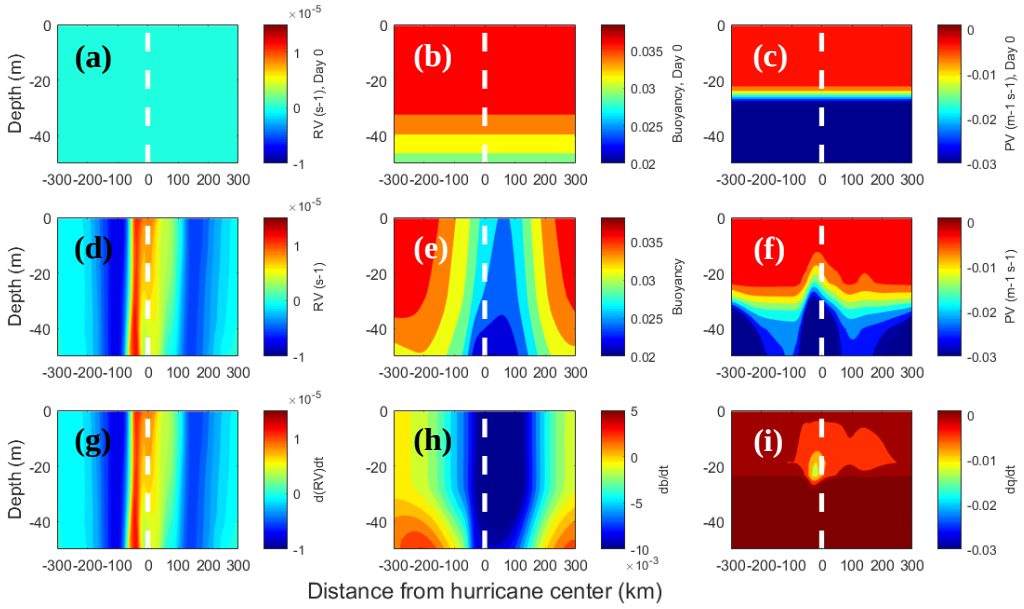

Fig. 11 Case 1 zonally-averaged (a) relative vorticity (RV), (b) buoyancy (m s^{-2}), and (c) potential vorticity (PV) at day 0. Zonally- and time-averaged (d) RV, (e) buoyancy, and (f) PV from days 1 to 6.8, and the change over time between the two rows (g-i). Variables have been zonally averaged over the black box in Fig. 2. The white dashed lines indicate the hurricane center, and the view is westward in the direction of the translating hurricane

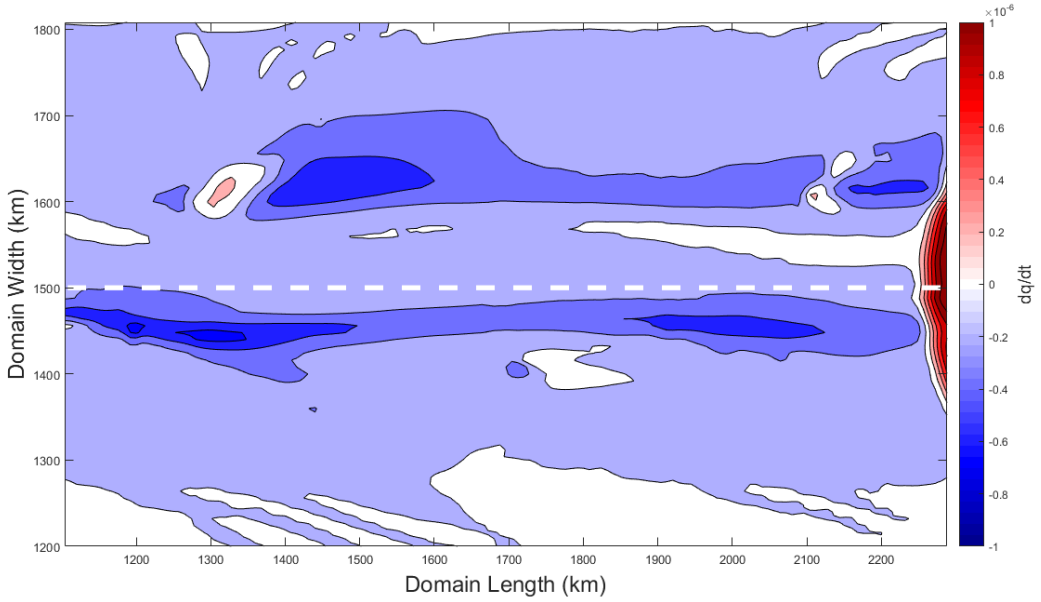

Fig. 12 Surface change in PV (dq/dt) over the black box in Fig. 2, time-averaged for three inertial periods from days 1 to 6.8. The white dashed line indicates the hurricane center

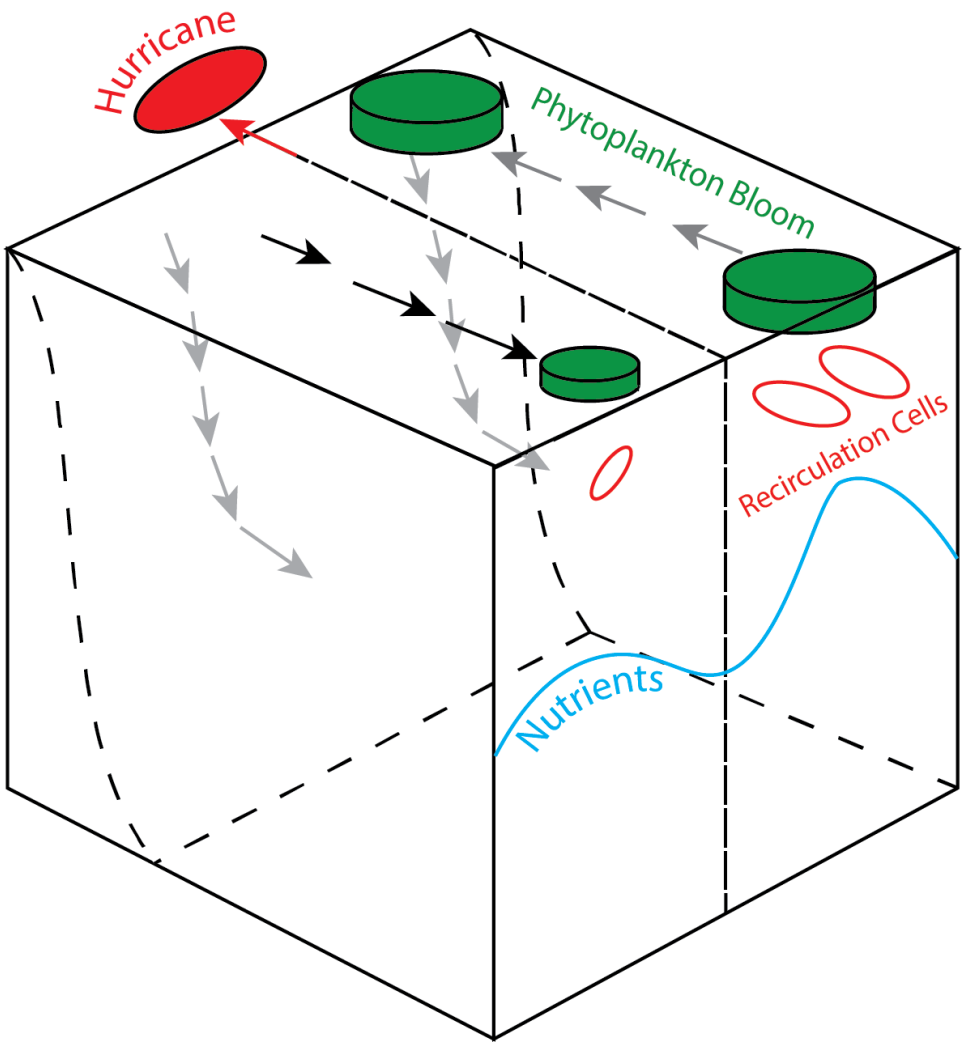

Fig. 13 Conceptual model of processes leading to right-side bloom asymmetry in Cases 1 and 2. Circulation direction is indicated by arrows, with depth indicated by shading (darkest at the surface, lightest at depth)